Charge transport through spin-polarized tunnel junction between two spin-split superconductors

Mikel Rouco,[1,*] Subrata Chakraborty,[2,3,†] Faluke Aikebaier,[2] Vitaly N. Golovach,[1,4,5] Elia Strambini,[6] Jagadeesh S. Moodera,[7] Francesco Giazotto,[6,‡] Tero T. Heikkilä,[2,§] and F. Sebastian Bergeret[1,5,‖]

[1]*Centro de Física de Materiales (CFM-MPC), Centro Mixto CSIC-UPV/EHU, Manuel de Lardizabal 5, E-20018 San Sebastián, Spain*

[2]*Department of Physics and Nanoscience Center, University of Jyväskylä, P.O. Box 35 (YFL), FI-40014 Jyväskylä, Finland*

[3]*Department of Physics, Queens College of the City University of New York, Queens, New York 11367, USA*

[4]*IKERBASQUE, Basque Foundation for Science, 48013 Bilbao, Basque Country, Spain*

[5]*Donostia International Physics Center (DIPC), Manuel de Lardizabal 4, E-20018 San Sebastian, Spain*

[6]*NEST Istituto Nanoscienze-CNR and Scuola Normale Superiore, I-56127 Pisa, Italy*

[7]*Department of Physics and Francis Bitter Magnet Lab, Massachusetts Institute of Technology, Cambridge, Massachusetts 02139, USA*

(Received 21 June 2019; revised manuscript received 1 October 2019; published 4 November 2019)

We investigate transport properties of junctions between two spin-split superconductors linked by a spin-polarized tunneling barrier. The spin-splitting fields in the superconductors (S) are induced by adjacent ferromagnetic insulating (FI) layers with arbitrary magnetization. The aim of this study is twofold. On the one hand, we present a theoretical framework based on the quasiclassical Green's functions to calculate the Josephson and quasiparticle current through the junctions in terms of the different parameters characterizing it. Our theory predicts qualitative new results for the tunneling differential conductance, dI/dV, when the spin-splitting fields of the two superconductors are noncollinear. We also discuss how junctions based on FI/S can be used to realize anomalous Josephson junctions with a constant geometric phase shift in the current-phase relation. As a result, they may exhibit spontaneous triplet supercurrents in the absence of a phase difference between the S electrodes. On the other hand, we show results of planar tunneling spectroscopy of a EuS/Al/AlO_x/EuS/Al junction and use our theoretical model to reproduce the obtained dI/dV curves. Comparison between theory and experiment reveals information about the intrinsic parameters of the junction, such as the size of the superconducting order parameter, spin-splitting fields and spin relaxation, and also about properties of the two EuS films, such as their morphology, domain structure, and magnetic anisotropy.

DOI: 10.1103/PhysRevB.100.184501

I. INTRODUCTION

Superconducting films with spin-split density of states have been used for a long time to determine the spin polarization of ferromagnetic metals tunnel-coupled to the superconductor (S) [1–7]. Originally, the spin splitting was induced by applying in-plane magnetic fields to thin superconducting films. These fields had to be large, of the order of few tesla, in order to obtain sizable splittings. Interestingly, as shown in the late 1980s, such spin splitting can also be observed at rather small, or even zero, magnetic fields in superconducting Al layers adjacent to ferromagnetic insulators (FI) [8,9]. In this case, the splitting is attributed to the exchange interaction at the FI/S interface [10]. Additionally, those first works on FI/S structures showed that thin FI layers can also be used as very efficient spin filters, with potential application as sources for highly spin-polarized spin currents [11].

More recently, nonequilibrium properties of superconductors with a spin-split density of states have attracted a renewed attention [12–18]. In such systems, two additional spin-dependent modes appear and couple to the widely studied nonequilibrium energy and charge modes [16,19]. FI/S structures have also been suggested for several applications, as highly efficient thermoelectric elements [20,21], bolometers [22], thermometers [23], cryogenic RAM memories [24], and different caloritronic devices to access the electronic heat current in nanostructures [25–29].

Most of these applications require both superconductors with spin-split density of states and highly polarized spin-filter interfaces. This motivates the present work, in which we explore both theoretically and experimentally FI/S junctions. Theoretically, we develop a general model to describe the coupling of two spin-split superconductors through an additional spin-filter barrier. Our model takes into account self-consistently magnetic disorder, spin-orbit coupling, and orbital effects of the magnetic field, as well as noncollinear spin-splitting fields. On the one hand, our model predicts new features in FI/S-based junctions: Additional coherent peaks in the differential conductance when the FI layers are monodomain with noncollinear magnetization, and the possible realization of an anomalous Josephson junction with pure triplet supercurrents at zero phase bias. On the other hand, our model provides a tool to interpret transport experiments on tunneling junctions with FI/S electrodes.

*mikel.rouco@ehu.eus
†schrkmv@gmail.com
‡francesco.giazotto@sns.it
§tero.t.heikkila@jyu.fi
‖fs.bergeret@csic.es

Experimentally, we measure the tunneling conductance of an EuS/Al/AlO_x/EuS/Al junction as a function of the applied voltage and magnetic field. The differential tunneling conductance, dI/dV, shows sharp peaks whose heights depend on the effective spin splitting induced in both Al layers and the spin filtering of the barrier. Below, we perform a self-consistent calculation that allows us to determine unambiguously the main parameters governing the transport of the junction

The work is organized as follows. In the next section, we present the measurements of the tunneling conductance of the junction under consideration as a function of the magnetic field. In Sec. III, we present a theoretical model based on the quasiclassical Green's functions for the description of the transport properties of a generic FI/S/I/FI/I/S/FI junction. In Sec. IV, we discuss the Josephson current through such junctions with emphasis on the anomalous behavior when the FI magnetizations are noncollinear. In Sec. V, we focus on the quasiparticle current and the tunneling differential conductance. The latter is compared to the experimental data, and a discussion of the results follows. We present our conclusions in Sec. VI.

II. TUNNELING CONDUCTANCE OF A EuS/Al/AlO_x/EuS/Al JUNCTION

In this section, we present our measurements of the current-voltage (I-V) characteristic of a EuS(4)/Al(4)/AlO_x/EuS(1.2)/Al(4.3)[1] junction (thickness in nanometers), see inset in Fig. 1(a). The samples consist of cross bars fabricated by electron-beam evaporation on an in situ metallic shadow mask with a typical junction area of $290 \times 290\ \mu m^2$ [30].

The tunneling spectroscopy is obtained by measuring the I-V characteristic in a dc two-wire setup, as sketched in the inset of Fig. 1(a). From this measurement we determine the differential conductance, dI/dV, via numerical differentiation. The measurements are done at cryogenic temperatures in a filtered cryogen-free dilution refrigerator. We first cool down the sample from room temperature to 25 mK in a nonmagnetic environment. Before applying any external magnetic field, we measure the I-V characteristic [Fig. 1(a)] and extract the dI/dV shown by the solid line in Fig. 1(b). We then apply an in-plane magnetic field (up to 160 mT) strong enough to align the magnetization of both EuS layers, and start decreasing it. During this process, we measure the I-V characteristic and determine the tunneling conductance at each value of the applied magnetic field. The full dependence is shown in the color plot of Fig. 2(d). Panels (a)–(c) in Fig. 2 correspond to different vertical cuts of Fig. 2(d) at the positions indicated by the arrows placed at the bottom of the figure.

The obtained tunneling conductance clearly shows the four-peak structure expected from the spin-split superconducting density of states (DOS) [9]. Notice that these peaks are also observed before applying any magnetic field, Fig. 1(b). The position of the peaks in Figs. 2(a)–2(c) is always symmetric with respect to the sign of the applied voltage, however, after the first magnetization of the junction, their heights are not. This behavior contrasts with the one shown in Fig. 1(b) for the demagnetized sample. The asymmetry is a fingerprint of spin-polarized tunneling through the middle EuS thin layer

[1]During growth, the oxidation of the aluminum layer was not controlled. Therefore it does not necessarily have the stoichometry of Al_2O_3.

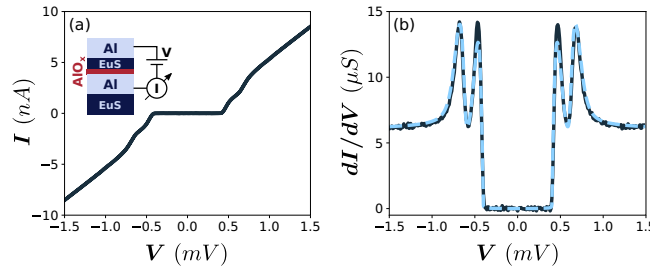

FIG. 1. Tunneling spectroscopy of a FI/S/I/FI/S junction before applying an external magnetic field. (a) Typical current (I) vs voltage (V) characteristic of the junction measured at 25 mK. (b) Numerical derivative of the I-V characteristic extracted from the data in (a) (black line). The blue dashed line is obtained from our theoretical model presented in Sec. III. The parameters used for the fitting are: $G_T = 6\ \mu$S, $\Delta_0 = 320\ \mu$eV, $h_L = 0$, $h_R = 100\ \mu$eV, $\tau_{sf}^{-1} = 0.08\Delta_0$, and $\tau_{so}^{-1} = \tau_{orb}^{-1} = 0$. In the demagnetized regime, the effective spin splitting in the upper Al layer is negligibly small. The spin splitting arises from the very large domain structure of the bottom EuS layer, with size much larger than the superconducting coherence length ξ_0. The measured peak structure resembles the one measured in Ref. [30] without the spin-filtering effect at work [see discussion after Eq. (37) for more details].

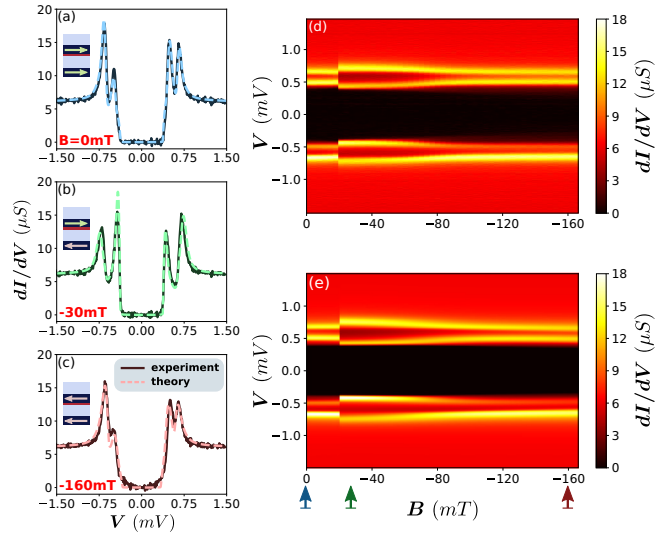

FIG. 2. Magnetic-field dependence of the tunneling conductance of the spin-polarized junction. Before the measurement, the system is polarized with a positive magnetic field ($B = 160$ mT). The differential conductance is then measured at different values of magnetic fields from 0 to -160 mT. (a), (b), and (c) show three different curves measured at 0, -20, and -160 mT, respectively. (d) shows the full measured B dependence. (e) is the fitting resulting from the theoretical model.

[7–9], which only after magnetization turns out to be apparent. In contrast, and according to the physical picture provided in Sec. V, when the sample is demagnetized, the thin EuS barrier layer consists of magnetic domains smaller than the coherence length with random polarization directions. This leads to a negligibly small value of the induced spin-splitting field on the upper superconductor and no spin-filtering effect on the current after averaging over the junction area.

The separation between the peaks at positive (or negative) voltage, Figs. 1(b) and 2(a)–2(c), provides information about the size of the spin-splitting energy induced in the Al layers. This splitting is proportional to the effective exchange energy between the spins localized at the EuS/Al interface and the Al conduction electrons [31].

We observe a sudden increase of the spin-splitting energy at -20 mT [Fig. 2(d)], which occurs when the system switches to the antiparallel configuration. As it turns out from our theoretical discussion in Sec. V, it is the bottom EuS layer that switches first and abruptly. By further increasing the magnetic field B the parallel configuration is recovered gradually with a smooth switching of the middle EuS magnetization. The two rather different switching behaviors of the EuS films can be attributed to a different magnetic configuration and anisotropy of the two films due to different deposition conditions, which crucially depends on the growth morphology [24,32].

Whereas the peak positions can be explained by using a simple tunneling model [7], detailed features such as the width and height of the peaks can only be understood by taking into account different scattering and depairing mechanisms and performing a self-consistent calculation of the superconducting order parameter. With this aim, in the next sections we present a theoretical model that allows us to describe the dI/dV curves, extract the values of the different parameters, and provide a physical picture that explains the full behavior shown in Fig. 2(d).

III. THE MODEL

In this section, we present a theoretical model to describe the electronic transport in junctions with spin-split superconductors and spin-filtering barriers. The goal of this section is twofold. On the one hand, to obtain general results for the current in tunnel junctions between two spin-split superconductors in the presence of a spin-filtering barrier. On the other hand, we provide a complete description of the experimental results presented in the previous section.

We consider a generic junction, sketched in Fig. 3. It consists of two spin-split superconductors separated by a spin-polarized tunneling barrier. The spin-split superconductors correspond to two S/FI bilayers, whereas the tunneling barrier is an additional FI layer with adjacent thin insulating layers to decouple it magnetically from the superconductors.

To describe the current through the junction below, we use the tunneling Hamiltonian approach, such that the system is described by

$$H = H_L + H_R + H_T . \tag{1}$$

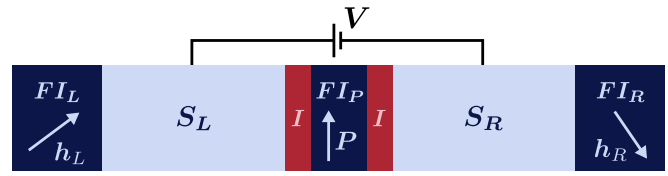

FIG. 3. Schematic of a tunnel junction between two spin-split superconductors with a spin polarized tunneling barrier and biased at a voltage V. The left (right) superconductor S_L (S_R) experiences a spin-splitting field $\boldsymbol{h}_L$ ($\boldsymbol{h}_R$) by an attached ferromagnetic insulator layer FI_L (FI_R). The spin polarized tunneling barrier, with polarization $\boldsymbol{P}$, is another ferromagnetic insulator (FI). To avoid the magnetic proximity effect, the superconductors are separated from the spin-polarized tunneling barrier by insulating layers (I). The superconductor S_L (S_R) is at temperature T_L (T_R).

Here, $H_{L(R)}$ describes the left(right) superconducting electrode attached to a FI and H_T the tunneling of electrons between the superconductors [33].

In order to compute the current one needs to determine the spectral properties of the decoupled FI-S electrodes. We model them by assuming that the interaction between the localized magnetic moments in the FI and the conduction electrons in the S layer creates an effective exchange field in the latter [18,31,34,35]. If the superconducting films are thinner than the coherence length such exchange field can be assumed to be homogeneous in the S and, hence, the S electrodes are described by

$$H_{L(R)} = H_{\rm BCS} + \mathbf{h}_{L(R)} \cdot \hat{\boldsymbol{\sigma}} , \tag{2}$$

where $\mathbf{h}_{L(R)} = h_{L(R)}\mathbf{n}_{L(R)}$ is the exchange field pointing in the direction of the unit vector $\mathbf{n}_{L(R)}$, $\hat{\boldsymbol{\sigma}}$ is the vector of Pauli matrices and $H_{\rm BCS}$ is the BCS Hamiltonian that also includes random impurities, magnetic, nonmagnetic, and those with spin-orbit coupling [36].

For the tunneling Hamiltonian [the last term of Eq. (1)] we assume that the tunneling through the barrier is spin dependent; in other words, that the electron tunneling probability depends on whether its spin is oriented parallel or antiparallel with respect to the barrier magnetization [37].

We consider a general case where the directions of the magnetization in each of the three FIs are independent of each other. A voltage V is applied across the junction and, in principle, the temperatures of the two FI/S electrodes are different $T_L \neq T_R$. Here, the indices L and R denote the left and right electrodes, respectively.

The effective splitting of the left and right superconductors in Fig. 3 is given by the induced exchange fields $\boldsymbol{h}_L = h_L\boldsymbol{n}_L$ and $\boldsymbol{h}_R = h_R\boldsymbol{n}_R$, respectively, whereas the spin filtering is described by the polarization vector $\boldsymbol{P} = P\boldsymbol{n}_P$ with $P \equiv \frac{G_\uparrow - G_\downarrow}{G_\uparrow + G_\downarrow}$ and $0 \leqslant P \leqslant 1$. The vectors $\boldsymbol{n}$ are unit vectors pointing in the respective directions, the magnitude of the exchange fields $h_{L/R}$ has energy units and $G_{\uparrow(\downarrow)}$ stands for the tunneling conductance through the junction for carriers with up (down) spin along the direction of $\mathbf{n}_P$.

Without loss of generality, we set the barrier magnetization along the z axis, $\boldsymbol{n}_P = (0, 0, 1)$, such that the magnetization orientations of the adjacent S/FI bilayers can be parametrized

by three angles, $\theta_{L,R}$ and γ:

$$\boldsymbol{n}_L = (\sin\theta_L, 0, \cos\theta_L) \tag{3}$$

and

$$\boldsymbol{n}_R = (\sin\theta_R\cos\gamma, \sin\theta_R\sin\gamma, \cos\theta_R). \tag{4}$$

In a collinear configuration, i.e., $\theta_L = \theta_R = 0$, the current through the junction can be straightforwardly calculated from the well-known tunneling expression [7]. We next generalize the latter for noncollinear magnetizations. Moreover, in order to include the effects of spin relaxation and depairing, we use the quasiclassical Green's functions (GFs) for an accurate description of the spectrum of the S/FI electrodes.

A. Quasiclassical Green's functions for spin-split superconductors

In this section, we present the quasiclassical Green's functions and the expression for the current as a function of the applied voltage and temperature bias (see also Ref. [18]) for an arbitrary magnetic configuration of the junction shown in Fig. 3. We restrict our analysis to the tunneling limit, which corresponds to the experimental situation when a FI is used as a barrier. In such case, one can treat each FI/S electrode in Fig. 3 independently. In other words, we can calculate the GFs, $\check{g}_L(\epsilon)$ and $\check{g}_R(\epsilon)$, for each electrode. Moreover, one can first consider the case in which $V = 0$ and $\varphi = 0$, where φ is the phase difference between the superconductors. Finite φ and V can then be added as gauge factors.

We use the Green's functions defined in the Keldysh⊗Nambu⊗spin space.[2] These are are 8×8 matrices that satisfy the normalization condition

$$\check{g}_s^2 = 1\,. \tag{5}$$

In the Keldysh space, they can be written as [38]

$$\check{g}_s = \begin{pmatrix} \check{g}_s^R & \check{g}_s^K \\ 0 & \check{g}_s^A \end{pmatrix}, \tag{6}$$

where $s = \{L, R\}$ labels left and right sides of the junction, $\check{g}_s^R$ stands for the retarded component of the GFs, $\check{g}_s^A = -\hat{\tau}_3\check{g}_S^{R\dagger}\hat{\tau}_3$ is the advanced component, and due to the normalization condition, the Keldysh component can be written as

$$\check{g}_s^K = \check{g}_s^R\check{f}_s - \check{f}_s\check{g}_s^A. \tag{7}$$

In these expressions, the "checks" $\check{\cdot}$ indicate the full 8×8 matrices, whereas $\hat{\cdot}$ are used for 4×4 matrices in Nambu spin space, and $\hat{\cdot}$ for 2×2 matrices. $\hat{\tau}_i$ is the ith Pauli matrix in Nambu space and $\hat{f}_s$ stands for the electron distribution function in electrode s. In equilibrium, the latter is proportional to the unit matrix in Nambu and spin space and reads

$$\check{f}_s(\epsilon) \equiv f_0(\epsilon, T_s) = \tanh\frac{\epsilon}{2k_BT_s}, \tag{8}$$

where k_B is the Boltzmann's constant and T_s is the temperature on the s side of the junction. In our notation, whenever we do not specify any matrix structure via Pauli matrices, it is implied that the matrix is proportional to the unit matrix in the corresponding space.

We now calculate the GFs in the electrodes, which we assume in thermal equilibrium. In the diffusive limit, they obey the Usadel equation [39] with a local spin splitting pointing in z direction and, as it was indicated after Eq. (6) and in Eq. (7), we only need to compute their retarded component. Then, to calculate the current through the junction with noncollinear magnetizations we will have to transform the GFs by using spin-rotation operators.

The Usadel equation for the retarded component of a homogeneous S/FI electrode in the spin local frame reads

$$\left[i\epsilon\hat{\tau}_3 - ih_s\hat{\tau}_3\hat{\sigma}_3 - \Delta_s\hat{\tau}_1 - \check{\Sigma}_s,\ \check{g}_s^R\right] = 0, \tag{9}$$

where $\hat{\sigma}_i$ is the ith Pauli matrix in the spin space and Δ_s is the self-consistent superconducting order parameter (see Appendix A for details). The self-energy $\check{\Sigma}_s$ consists of three contributions:

$$\check{\Sigma}_s = \check{\Sigma}_s^{\rm so} + \check{\Sigma}_s^{\rm sf} + \check{\Sigma}_s^{\rm orb}, \tag{10}$$

the spin relaxation due to spin-orbit coupling, $\check{\Sigma}_s^{\rm so}$, and spin-flip relaxation, $\check{\Sigma}_s^{\rm sf}$, and the orbital depairing, $\check{\Sigma}_s^{\rm orb}$, due to the external magnetic fields. Explicitly, each contribution within the relaxation time approximation reads

$$\check{\Sigma}_s^{\rm so} = \frac{\hat{\boldsymbol{\sigma}}\cdot\check{g}_s^R\cdot\hat{\boldsymbol{\sigma}}}{8\tau_s^{\rm so}}, \tag{11}$$

$$\check{\Sigma}_s^{\rm sf} = \frac{\hat{\boldsymbol{\sigma}}\cdot\hat{\tau}_3\check{g}_s^R\hat{\tau}_3\cdot\hat{\boldsymbol{\sigma}}}{8\tau_s^{\rm sf}}, \tag{12}$$

$$\check{\Sigma}_s^{\rm orb} = \frac{\hat{\tau}_3\check{g}_s^R\hat{\tau}_3}{\tau_s^{\rm orb}}, \tag{13}$$

where $\tau_s^{\rm so}$, $\tau_s^{\rm sf}$, and $\tau_s^{\rm orb}$ stand for spin-orbit, spin-flip, and orbital depairing relaxation times, respectively, and we use the notation $\hat{\boldsymbol{\sigma}}\cdot\check{A}\cdot\hat{\boldsymbol{\sigma}} = \sum_{i=1}^3\hat{\sigma}_i\check{A}\hat{\sigma}_i$.

The general solution of the Usadel equation (9), is then given by four components in the Nambu spin space:

$$\check{g}_s^R = (F_{0s} + F_{3s}\hat{\sigma}_3)\hat{\tau}_1 + (G_{0s} + G_{3s}\hat{\sigma}_3)\hat{\tau}_3. \tag{14}$$

The components proportional to τ_3 are the normal components. They determine the quasiparticle spectrum and enter the expression for the quasiparticle current. The off-diagonal terms in Nambu space, here proportional to τ_1, are the anomalous GFs and describe the superconducting condensate. They determine the Josephson current through the junction of Fig. 3. The anomalous GFs have two components: F_{0s} describes the singlet condensate, whereas the component F_{3s} describes the triplet component with zero total spin projection. Because we are considering diffusive systems, both components have s-wave symmetry. This implies that the triplet component is odd in frequency [40]. In Sec. V, we numerically solve the Usadel equation, Eq. (9), together with the normalization condition, Eq. (5), and the self-consistent expression for Δ_s (see Appendix A).

We next derive the expression for the tunneling current in terms of the above GFs.

[2]To simplify the notation we skip throughout the text the direct product symbol ⊗.

B. Tunneling current

In the previous section, we present the quasiclassical GFs, $\check{g}_s(\epsilon)$, in a local reference frame where $V = 0$, $\varphi = 0$ and the exchange field is parallel to the z axis. We now use these results to calculate the total electric current across the Josephson junction, sketched in Fig. 3, in the presence of a finite voltage and phase difference, and a noncollinear magnetic configuration. This can be done by a gauge transformation and a spin-rotation of the GFs.

In the presence of a voltage, the phase of a superconductor evolves in time as

$$\varphi(t) = \varphi + \frac{2eV}{\hbar} t \ , \tag{15}$$

where φ is the dc phase. We define the corresponding gauge matrix

$$\hat{U}(t) = \exp(-i\varphi(t)\hat{\tau}_3) \ . \tag{16}$$

If we assume that the voltage is applied on the left superconductor and the magnetizations of the two S/FI and the spin-filter barrier are noncollinear [see Eqs. (3) and (4)], we can obtain the GFs $\check{\tilde{g}}$ from those obtained in in Sec III A via the following transformations:

$$\check{\tilde{g}}_L(t-t') = \hat{R}_L \, \hat{U}(t) \, \check{g}_L(t-t') \, \hat{U}(t')^\dagger \, \hat{R}_L^\dagger, \tag{17}$$

$$\check{\tilde{g}}_R(t-t') = \hat{R}_R \, \check{g}_R(t-t') \, \hat{R}_R^\dagger. \tag{18}$$

Here, the operators $\hat{R}_s$ describe spin rotations in the left and right electrodes:

$$\hat{R}_L = \exp(-i\theta_L \hat{\sigma}_y/2), \tag{19}$$

$$\hat{R}_R = \exp(-i\gamma\hat{\sigma}_z/2)\exp(-i\theta_R\hat{\sigma}_y/2) \ , \tag{20}$$

and the time-dependent Green's functions in Eqs. (19) and (20) are obtained from the GFs in frequency space:

$$\check{g}_s(t-t') = \frac{1}{2\pi}\int_{-\infty}^{\infty} d\epsilon \ \check{g}_s(\epsilon) \ e^{i\epsilon(t-t)} \ . \tag{21}$$

From Eqs. (17) and (18), we can now write the full expression for the time-dependent electric current across the junction shown in Fig. 3 [41]:

$$I_c(t) = \frac{G_T \pi}{16e} \, \mathrm{Tr}(\hat{\tau}_3[\check{\tilde{g}}_L \circ \check{\Gamma}\check{\tilde{g}}_R\check{\Gamma}]^K), \tag{22}$$

where G_T is the normal state conductance of the junction, $[\cdot \circ \cdot]$ is a commutator of convolutions,[3] the superscript K stands for the Keldysh component of the commutator, and Tr stands for the trace over the Nambu×spin spaces.

[3] When the operators depend only on the difference of times the convolution is defined as

$$(A \circ B)(t) = \int_{-\infty}^{\infty} dt' A(t-t')B(t'-t).$$

Consequently, the commutator reads

$$[A \, ; B] = (A \circ B)(t) - (B \circ A)(t).$$

Equation (22) is valid in the tunneling limit. The matrix $\check{\Gamma}$ describes the effect of the spin-filtering layer and is defined as

$$\check{\Gamma} = u + v\hat{\sigma}_3\hat{\tau}_3 \ , \tag{23}$$

where the parameters u and v depend on the polarization of the barrier P as follows:

$$u = \sqrt{\frac{1+\sqrt{1-P^2}}{2}}, \tag{24}$$

$$v = \sqrt{\frac{1-\sqrt{1-P^2}}{2}}. \tag{25}$$

One can easily check from these expressions that $u^2 + v^2 = 1$, $2uv = P$, and $u^2 - v^2 = \sqrt{1-P^2}$.

After a lengthy but straightforward algebra, we obtain from Eq. (22) the charge current through the junction which can be written as the sum of three components:

$$I_c(t) = I + J_1 \sin\left(\varphi + \frac{2eVt}{\hbar}\right) + J_2 \cos\left(\varphi + \frac{2eVt}{\hbar}\right). \tag{26}$$

Here, I is the quasiparticle tunneling current and the remaining part is the Josephson current. Specifically, J_1 is the usual Josephson critical current. The third term is proportional to the cosine of $\varphi(t)$. In a nonmagnetic Josephson junction, this term is finite only at nonzero bias. In the literature, it is known as the $\cos\varphi$ term and has been widely studied [42–44]. Interestingly, in a magnetic junction, this term can be nonzero even when $V = 0$. In this case, this term leads to the so-called anomalous Josephson current that appears in certain magnetic system with spin-orbit coupling or inhomogeneous magnetization [45–55] and is discussed in more detail in Sec. IV.

From Eq. (22), we derive the expressions for the three components of the current in terms of the GFs. For the quasiparticle tunneling current, first term in Eq. (26), we obtain

$$\begin{aligned} I = \frac{G_T}{2e}\int_{-\infty}^{\infty} d\epsilon [f_0(\epsilon+eV,T_L) - f_0(\epsilon,T_R)] \\ \times \{P[\mathcal{N}_{0L}(\epsilon+eV)\mathcal{N}_{3R}(\epsilon)\boldsymbol{n}_R\cdot\boldsymbol{n}_P \\ + \mathcal{N}_{3L}(\epsilon+eV)\mathcal{N}_{0R}(\epsilon)\boldsymbol{n}_L\cdot\boldsymbol{n}_P] \\ + \mathcal{N}_{0L}(\epsilon+eV)\mathcal{N}_{0R}(\epsilon) + \mathcal{N}_{3L}(\epsilon+eV)\mathcal{N}_{3R}(\epsilon) \\ \times [\boldsymbol{n}_L^\parallel\cdot\boldsymbol{n}_R^\parallel + \sqrt{1-P^2}\,\boldsymbol{n}_L^\perp\cdot\boldsymbol{n}_R^\perp]\}, \end{aligned} \tag{27}$$

where $\mathcal{N}_{is}(\epsilon) \equiv \mathrm{Re}[G_{is}(\epsilon)]$ is the semisum ($i = 0$) and semidifference ($i = 3$) of the spin-up/spin-down densities of states (DOS). In deriving this expression we have used the vector equalities presented in Appendix B.

For the second and third terms in Eq. (26), we obtain

$$\begin{aligned} J_1 = A_0\sqrt{1-P^2} + A_3[\sqrt{1-P^2}\,\boldsymbol{n}_L^\parallel\cdot\boldsymbol{n}_R^\parallel \\ + \boldsymbol{n}_L^\perp\cdot\boldsymbol{n}_R^\perp] - B_3\,P\boldsymbol{n}_P\cdot(\boldsymbol{n}_L\times\boldsymbol{n}_R) \end{aligned} \tag{28}$$

and

$$\begin{aligned} J_2 = B_0\sqrt{1-P^2} + B_3[\sqrt{1-P^2}\,\boldsymbol{n}_L^\parallel\cdot\boldsymbol{n}_R^\parallel \\ + \boldsymbol{n}_L^\perp\cdot\boldsymbol{n}_R^\perp] + A_3\,P\boldsymbol{n}_P\cdot(\boldsymbol{n}_L\times\boldsymbol{n}_R), \end{aligned} \tag{29}$$

where A_i and B_i ($i = 1, 3$) are expressed in terms of the real and imaginary parts of the anomalous GFs $F_{is}(\epsilon)$:

$$A_i = \frac{G_T}{2e}\int_{-\infty}^{\infty} d\epsilon [f_0(\epsilon, T_R)\mathrm{Re}[F_{iL}(\epsilon + eV)]\mathrm{Im}[F_{iR}(\epsilon)] + f_0(\epsilon + eV, T_L)\mathrm{Im}[F_{iL}(\epsilon + eV)]\mathrm{Re}[F_{iR}(\epsilon)]], \quad (30)$$

$$B_i = \frac{G_T}{2e}\int_{-\infty}^{\infty} d\epsilon [f_0(\epsilon + eV, T_L) - f_0(\epsilon, T_R)] \times \mathrm{Im}[F_{iL}(\epsilon + eV)]\mathrm{Im}[F_{iR}(\epsilon)]. \quad (31)$$

Equations (26)–(31) determine the total current through the junction and are used in the next sections. We start by analyzing the Josephson current in magnetic junctions.

IV. ANOMALOUS JOSEPHSON CURRENT

An interesting situation occurs when $V = 0$, $\varphi = 0$, $T_L = T_R$ and the magnetization vectors of the three FI layers are not in the same plane. In this case, $I = 0$, $B_0 = B_3 = 0$ and the only term contributing to the current J_2 is the one proportional to A_3 in Eq. (29). The latter is finite when $\boldsymbol{n}_P \cdot (\boldsymbol{n}_L \times \boldsymbol{n}_R) \neq 0$, i.e., when three vectors are not coplanar. In this case a finite Josephson current may flow through the junction even if the dc phase difference φ is zero. This is the so-called anomalous Josephson current and the junction is referred as a φ_0 junction. The latter has been widely studied in magnetic junctions with spin-orbit coupling [45,50,51,53,56–58] or multilayer metallic ferromagnets [54,55,59–64].

In this section, we discuss the possible observation of the anomalous Josephson junction in FI/S-based junctions. This effect was not yet seen in the samples discussed here, because the large value of the normal-state resistance made it impossible to measure any Josephson current at the temperature of the experiments. However, similar type of samples with increased junction transparency would be good candidates for measuring the anomalous φ_0 effect.

Because we assume a unique temperature, $T_L = T_R = T$, and the junction is in equilibrium ($V = 0$), quasiparticle current is zero and one can write the expression for the Josephson current in terms of a sum over Matsubara frequencies. The anomalous functions proportional to the Pauli matrix σ_3 correspond to the odd-in-frequency triplet components of the condensate, $F_3(i\omega_n) = -F_3(-i\omega_n)$, whereas those proportional to σ_0 arise from the singlet components $F_0(i\omega_n) = F_0(-i\omega_n)$ [65]. The total current, Eq. (26), can then be written as

$$J_1 = \pi T \frac{\pi G_T}{2e}\sum_{\omega}\left[\sqrt{1-P^2}\left(F_0^2 + F_3^2 \boldsymbol{n}_L^{\parallel}\cdot\boldsymbol{n}_R^{\parallel}\right) + F_3^2 \boldsymbol{n}_L^{\perp}\cdot\boldsymbol{n}_R^{\perp}\right], \quad (32)$$

$$J_2 = \pi T \frac{\pi G_T}{2e} P \boldsymbol{n}_P \cdot (\boldsymbol{n}_L \times \boldsymbol{n}_R)\sum_{\omega} F_3^2. \quad (33)$$

The contribution proportional to $\sin\varphi$ contains the conventional singlet Josephson current that vanishes when the barrier is fully polarized $P = 1$. If the magnetizations and the barrier magnetization are noncollinear, there is an additional contribution stemming entirely from the interference of the triplet component of the condensate, as discussed in Refs. [37,41].

The anomalous current in Eq. (33) is also a pure triplet current which requires noncoplanar vectors, i.e., a finite triple product $\boldsymbol{n}_P \cdot (\boldsymbol{n}_L \times \boldsymbol{n}_R)$, and it is proportional to the polarization of the barrier. The well-defined splitting and strong barrier polarization make the EuS/Al material combination suitable for the realization of such magnetic anomalous junctions.

In the limit $T \to 0$, we obtain analytic results for the Josephson current by assuming equal amplitudes of the exchange fields, $h_L = h_R \equiv h$, and neglecting all relaxation processes, $\tau_{\mathrm{so}}^{-1} = \tau_{\mathrm{sf}}^{-1} = \tau_{\mathrm{orb}}^{-1} = 0$:

$$J_1 = \frac{\pi G_T \Delta}{2e}[\sqrt{1-P^2}\eta + (\sqrt{1-P^2}\boldsymbol{n}_L^{\parallel}\cdot\boldsymbol{n}_R^{\parallel} + \boldsymbol{n}_L^{\perp}\cdot\boldsymbol{n}_R^{\perp})(\eta - 1)], \quad (34)$$

$$J_2 = \frac{\pi G_T \Delta}{2e} P(\eta - 1)\boldsymbol{n}_P \cdot (\boldsymbol{n}_L \times \boldsymbol{n}_R), \quad (35)$$

where Δ is the real self-consistent superconducting order parameter at zero temperature and exchange field h and

$$\eta \equiv \frac{32\Delta^2(256\Delta^4 - 32\Delta^2 h^2 + 9h^4)}{(16\Delta^2 - h^2)^3} - 1. \quad (36)$$

In the case where $h = 0$ (and, therefore, $\boldsymbol{n}_L = \boldsymbol{n}_R = 0$), the coefficient $\eta = 1$ and Eq. (34) yields the well-known Ambegaokar-Baratoff [66] formula for the Josephson current with a prefactor $\sqrt{1-P^2}$ due to the barrier polarization.

V. QUASIPARTICLE CURRENT AND DIFFERENTIAL CONDUCTANCE

In this section, we discuss the quasiparticle current, Eq. (27), and use our theoretical framework to describe the experimental data shown in Figs. 1 and 2. In the following discussion, we identify the layer at the bottom (top) in the experimental setup, Fig. 1, with the left (right) electrode of the model in Fig. 3.

The experimental setup corresponds to a situation in which the EuS barrier serves two purposes: On the one hand, it acts as a spin-filtering barrier and, on the other hand, it causes the spin splitting in one of the superconductors (the right one in Fig. 3). This means that the orientation of barrier magnetization coincides with the direction of the exchange field in the right superconductor, $\boldsymbol{n}_P = \boldsymbol{n}_R$, while the magnetization $\boldsymbol{n}_L$ is, in principle, independent of the magnetization of the barrier. The left superconductor (S_L) is in a good contact with the outer EuS, which induces a finite h_L. At the other interface between S_L and the tunneling barrier, a thin oxide layer is formed, preventing the exchange coupling [9]. Thus, for our specific sample, the thinnest FI layer in the middle is a tunneling barrier (1.2 nm) which induces the spin splitting only on the right superconductor and polarizes the current, whereas the thicker EuS layer (4 nm) causes the spin splitting in the left Al film.

Because the two EuS layers are of different thicknesses and they were grown on two different substrates, it is expected that the magnetization switching is different, as well as the strength of the induced exchange splittings in the superconductors, $h_R \neq h_L$. We assume the same superconducting order parameter, spin orbit and spin flip relaxation times for both

Al films. Moreover, the temperatures are assumed to be equal, $T_L = T_R = T$.

Because of the high normal-state resistance of the tunneling barrier (∼160 kΩ), no Josephson current through the junction could be measured, as shown in the left panel of Fig. 1. In particular, the Josephson energy $E_J = \hbar J_1/(2e)$ was of the order of the temperature and, therefore, the thermal fluctuations of the phase smeared out the Josephson effect. The current shown in that figure corresponds only to the quasiparticle contribution and it can be determined from Eq. (27) for $\boldsymbol{n}_R \cdot \boldsymbol{n}_P = 1$ and $\boldsymbol{n}_R^{\perp} = 0$. We can parametrize the magnetic configuration of the junction by a single angle θ between the splitting field in the left and right superconductor: $\boldsymbol{n}_R \cdot \boldsymbol{n}_L = \boldsymbol{n}_P \cdot \boldsymbol{n}_L = \cos\theta$.

From Eq. (27), we compute the current and, after differentiation with respect to V, we obtain the differential tunneling conductance dI/dV. In Fig. 4, we show its dependence on the voltage for different values of the angle θ and certain values of spin splitting fields and spin relaxation times. For a collinear configuration of magnetizations, $\cos\theta = \pm 1$, the differential conductance shows the four-peak structure, observed in most of experiments on EuS/Al based structures [7–9,30,67]. These peaks appear at voltages $eV = \pm(\Delta_L + \Delta_R) \pm (h_L - \cos\theta h_R)$.

However, if the magnetizations of the FIs are noncollinear, we find a qualitatively new result (see the solid black line in Fig. 4). Instead of four peaks, the differential conductance shows eight peaks for any value of θ between 0 and π. These two different behaviors can be understood as follows:

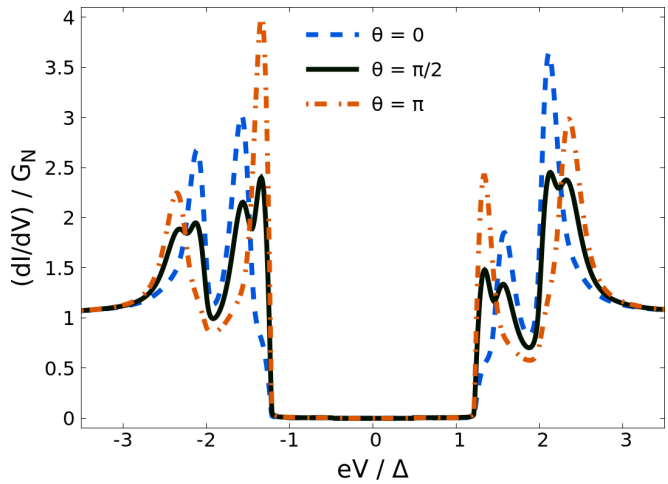

FIG. 4. Normalized differential conductance spectrum of the $FI_L/S_L/I/FI_R/S_R$ junction calculated from our theoretical model. Both superconductors are assumed to have the same order parameter, Δ_0. The polarization of the barrier is parallel to the exchange field induced in the right superconductor, $\boldsymbol{n}_P \parallel \boldsymbol{n}_R$, while the exchange field of the left superconductor forms an angle θ with $\boldsymbol{n}_R$. The dashed lines correspond to collinear situations, (blue) $\theta = 0$ and (red) $\theta = \pi$, while the solid black line corresponds to a noncollinear one, $\theta = \pi/2$. The remaining parameters used in the calculation are $\tau_{so}^{-1} = \tau_{orb}^{-1} = 0$ and $\tau_{sf}^{-1} = 0.08\Delta_0$ for the relaxation times in both superconductors, Zeeman splitting values of $h_L = 0.35\Delta_0$ and $h_R = 0.10\Delta_0$, a polarization of $P = 0.25$ and a global temperature of $k_B T = 0.01\Delta_0$.

In the collinear case, the spin component along the single direction of magnetization is globally conserved and the two spin species tunnel independently. When the polarization of the tunneling barrier is noncollinear with the magnetization of one of the electrodes, tunneling does not conserve spin. The additional peaks in the dI/dV stem from the projection of the electron spin of one of the electrodes onto the local spin basis in the other electrode. The peaks in dI/dV then appear at $eV = \pm(\Delta_L + \Delta_R) \pm (h_L \pm h_R)$

This unusual situation occurs when the induced exchange field, and hence the magnetization of the EuS films, is spatially homogeneous, so that the eight-peak structure of dI/dV shown in Fig. 4 can only be observed if the EuS are monodomain magnets with noncollinear magnetizations. In our EuS/Al samples the situation is rather different. As discussed in Ref. [30], EuS films consist of an ensemble of crystallites with intrinsic magnetization [68]. Therefore, before applying any external magnetic field, the magnetic configuration of the EuS layers consists of randomly oriented magnetic domains. Typically the size of EuS/Al tunnel junctions (here ∼290 × 290 μm^2) is much larger than the size of these domains and, therefore, the measured tunneling current is determined by an average over the angle θ, $\langle I \rangle_\theta \equiv \int_0^\pi \frac{d\theta}{\pi} I$, which reads

$$\langle I \rangle_\theta = \frac{G_T}{2e} \int_{-\infty}^{\infty} d\epsilon [f_0(\epsilon + eV, T_L) - f_0(\epsilon, T_R)] \times [\mathcal{N}_{0L}(\epsilon + eV)\mathcal{N}_{0R}(\epsilon) + P\mathcal{N}_{0L}(\epsilon + eV)\mathcal{N}_{3R}(\epsilon)]. \quad (37)$$

We use this averaging procedure to fit the experimental data shown in Fig. 1, which corresponds to the situation before any magnetic field has been applied. As discussed above, the finite spin-filtering coefficient P results in an asymmetry in the dI/dV curve with respect to the sign of V. However, Fig. 1 shows a quite symmetric curve. This can be explained by assuming that the domain size in the upper thin EuS layer is smaller than ξ_0 and, therefore, the possible splitting in the corresponding superconductor (R in our case) averages out. The absence of a Zeeman field in the right superconductor leads to an equal density of states for up and down electrons and, hence, $\mathcal{N}_{3R}(\epsilon) = 0$. Consequently, the second term on the second line of Eq. (37) does not contribute to the current, which now does not depend on the spin polarization of the tunneling barrier.

The theory curve in Fig. 1(b) (blue line), is obtained for $G_T = 6\,\mu S$, which is the value of the conductance measured at sufficiently large voltages (see the right panel of Fig. 1). The superconducting gap at zero field and zero temperature is set to $\Delta_0 = 320\ \mu$eV in both Al layers. According to previous studies on the spin relaxation processes in aluminum layers [17,69,70], we set the spin-orbit relaxation time to $\tau_{so}^{-1} = 0.005\Delta_0$. The spin-flip relaxation is however enhanced due to the magnetic disorder caused by the adjacent EuS layer and we chose $\tau_{sf}^{-1} = 0.08\Delta_0$ in both Al layers. Since the measurements in Fig. 1 are for zero field then $\tau_{orb}^{-1} = 0$. The best fitting is obtained for $h_L = 100\ \mu$eV (bottom layer in the experiment), whereas $h_R = 0$ as explained above. The EuS at the bottom is a thicker film and its magnetic domain size is of the order of, or even larger than, the superconducting

coherence length ξ_0 [30]. Therefore it induces a sizable exchange splitting in the bottom Al layer.

We now focus on the results of Fig. 2 when an external field is applied. These measurements are done after the first magnetization of EuS, i.e., after a strong enough in-plane magnetic field is applied ($B = 160$ mT). After this, we switched off the B-field and measured the I-V characteristic varying the magnetic field from $B = 0$ to $B \approx -160$ mT. The differential conductance obtained by a numerical differentiation is shown with solid lines in panels (a)–(c) of Fig. 2 for $B = 0$, $B = -30$ mT and $B = -160$ mT, respectively. A full overview of the dI/dV is presented as a color map in panel Fig. 2(d).

From the four-peak structure of dI/dV and the theoretical prediction in Fig. 4, we can conclude that the average induced exchange fields in the left and right superconductors are collinear. After the application of the initial strong magnetic field, the magnetizations of both EuS are aligned in the direction of B. By decreasing the field until it switches its direction, the magnetization of the FIs may also switch at their corresponding coercive fields leading to the usual ferromagnetic hysteresis loop. Such switching events can be seen from the evolution of the peak positions in the dI/dV map in Fig. 2(d).

We calculate the current using Eq. (27) and fit the data shown in Fig. 2. We use for the values of the spin-splitting fields for large magnetic fields (saturation of the magnetization of the EuS films) $h_L^{\rm sat} = 120$ μeV and $h_R^{\rm sat} = 30$ μeV. The difference between the values of the exchange fields after and before the first magnetization of the EuS layers is consistent with the result in Ref. [30]. In order to describe the evolution of the conductance peaks with the magnetic field, we assume that the exchange field follows the evolution of the local magnetization. In particular, for the color plot in Fig. 2(e), we assume that $h_L(B) = h_L^{\rm sat}\, y_L(B)$ and $h_R(B) = h_R^{\rm sat}\, y_R(B)$, whereas spin polarization of the barrier is chosen to be $P(B) = 0.25\, y_R(B)$. Here, $y_L(B) = 1 - 2\theta(B + 20)$ and $y_R(B) = \tanh \frac{B+70}{40}$ are two empirical functions that describe the evolution of the magnetization in the bottom and top EuS layers as a function of the magnetic field B given in mT, where $\theta(x)$ is the step function.

We also take into account the orbital depairing in the superconducting layers due to the applied magnetic field, determined by [71,72]

$$\tau_{\rm orb}^{-1} = \left(\frac{\pi d \xi_0 B}{\sqrt{6}\Phi_0}\right)^2 \Delta_0, \tag{38}$$

where Φ_0 is the magnetic flux quantum, $d \approx 4$ nm is the width of the Al layers and $\xi_0 \approx 200$ nm is the superconducting coherence length.

The results of our fitting procedure are the dashed lines in panels (a), (b), and (c) of Fig. 2 and the color map in panel (e). All in a good agreement with the experimental data.

At first glance our fitting suggests an unexpected behavior: The thin EuS layer switches its magnetization slower than the thicker one. Here we provide a plausible explanation for this behavior, which can be caused by the different polycrystalline structures of EuS layers grown under different conditions. The 4-nm-thick EuS (bottom layer in Fig. 2) is grown on an Al_2O_3 substrate, while the 1.2-nm barrier is grown directly on the previously oxidized underlying Al layer. As the oxidation of this layer is not controlled, its stoichiometry is completely different to the one on top of the substrate. Most likely, the thin layer consists of a more disordered set of crystallites and islands, resembling a superparamagnet. Such a large structural roughness could also arise from the propagation of defects created during growth in the bottom EuS and Al layers. If the RMS roughness is larger than half thickness of the top EuS layer, the layer would become discontinuous. Thus, the different thicknesses of the two EuS layers plays an important role in determining their magnetic properties as well. Presumably, the crystallites in the thick EuS layer are magnetically well coupled, while in the thin magnetic layer they form decoupled magnetic islands. Consequently, the EuS in the bottom would form magnetic domains on a scale much larger than the crystallite size, which leads to the sharp switching of the magnetization observed around $B = -20$ mT in Fig. 2(d). In the thin EuS layer, by contrast, the macroscopic magnetization is an average over the magnetization of the crystallites. Due to disorder, the anisotropy is also random and such crystallites would not switch simultaneously, resulting into the gradual magnetization reversal that we observe from $B \approx -60$ mT to ≈ -100 mT in Fig. 2(d). Moreover, the assumption of an island-like structure due to the growth morphology [32] can also explain the low polarization of the FI layer (25%) in comparison with previous results of near to 80% polarization [8,67]. Indeed, it seems that the coverage of the EuS barrier is not complete and, in addition to the spin polarized current, there is a parallel direct tunneling current through the AlO_x layer.

VI. CONCLUSIONS

We present an exhaustive analysis of tunnel junctions between spin-split superconductors coupled via a spin-polarized barrier. With the help of a theoretical model, we compute the spectral properties of the S/FI electrodes and determine the current through a FI/S/I/FI/I/S/FI junction, where the middle FI layer serves as a spin filter. Our theory predicts a previously unknown behavior of the differential tunneling conductance when the FI layers are noncollinear. Moreover, we suggest how to use these structures for the realization of so-called φ_0 junctions. In addition, our theory provides an accurate description of the differential conductance measurements of an EuS/Al/AlO_x/EuS/Al tunnel junction. We obtain diverse information from the comparison between theory and experiment. On the one hand we can determine the values for the induced spin-splitting fields, spin-filter efficiency, magnetic disorder, spin-orbit coupling, and orbital effects in the superconductors. On the other hand, from the magnetic field dependence of the $dI/dV(V)$ curves, we can extract information about the magnetic structure of the two EuS layers, which turns out to be very different due to the rather different growth morphology of each layer.

ACKNOWLEDGMENTS

This work was supported by EU's Horizon 2020 research and innovation program under Grant Agreement No. 800923 (SUPERTED). M.R., V.N.G., and F.S.B., acknowledge financial support by the Spanish Ministerio de Ciencia, Innovacion

y Universidades through the Projects No. FIS2014-55987-P and No. FIS2017-82804-P and by the grant "Grupos Consolidados UPV/EHU del Gobierno Vasco" (Grant No. IT1249-19). E.S. and F.G acknowledge partial financial support from the European Union's Seventh Framework Programme (FP7/2007-2013)/ERC Grant No. 615187- COMANCHE, and by the Tuscany Region under the FARFAS 2014 Project SCIADRO. S.C, F.A, and T.T.H. acknowledge support from the Academy of Finland (Key Funding Projects No. 305256 and No. 317118). The work of JSM at MIT was supported by NSF Grant No. DMR-1700137, ONR Grant No. N00014-16-1-2657, and ARO Grant No. W911NF1920041.

APPENDIX A: SELF-CONSISTENCY EQUATION

The superconducting gap for each superconductor in the paper is obtained self-consistently. In the quasiclassical theory, the self-consistency equation is given by

$$\Delta_s = \frac{\lambda}{16i}\int_{-\Omega_D}^{\Omega_D} d\epsilon \mathrm{Tr}\big[(\tau_1 - i\tau_2)\check{g}_s^K(\epsilon)\big], \tag{A1}$$

where $s = \{L, R\}$ labels the superconductor, λ is the coupling constant and Ω_D is the Debye cutoff energy. Using the expression for the Keldysh component in Eq. (7) and the parametrization of the Green's functions shown in Eq. (14), we can rewrite the self-consistency equation of the superconducting gap as

$$\Delta_s = \frac{\lambda}{2}\int_{-\Omega_D}^{\Omega_D} d\epsilon\ \mathrm{Im}[F_{0s}(\epsilon)]\tanh\left(\frac{\epsilon}{2k_BT}\right), \tag{A2}$$

We use this self-consistent superconducting gap, together with the Usadel equation in Eq. (9) to calculate the Green's functions used in current calculations.

APPENDIX B: RELATIONS BETWEEN UNIT VECTORS

In order to derive the expressions for the quasiparticle current and supercurrents in Sec. III, we made use of following relations between the unit vectors pointing in the direction of the polarization of the barrier, $\boldsymbol{n}_P$, and induced the exchange fields in the left, $\boldsymbol{n}_L$, and right, $\boldsymbol{n}_R$, electrodes. We define the parallel and perpendicular components of the exchange fields with respect to the polarization vector:

$$\boldsymbol{n}_s^{\parallel} \equiv (\boldsymbol{n}_s \cdot \boldsymbol{n}_P)\boldsymbol{n}_P = \cos\theta_s \boldsymbol{n}_P, \tag{B1}$$

$$\boldsymbol{n}_s^{\perp} \equiv \boldsymbol{n}_s - \boldsymbol{n}_s^{\parallel}, \tag{B2}$$

where $s = \{L, R\}$ labels the position of the electrode. According to these definitions and the expressions for the unit vectors of the Zeeman fields in Eqs. (3) and (4), we obtain the following useful relations:

$$\boldsymbol{n}_L \cdot \boldsymbol{n}_R = \boldsymbol{n}_L^{\parallel} \cdot \boldsymbol{n}_R^{\parallel} + \boldsymbol{n}_L^{\perp} \cdot \boldsymbol{n}_R^{\perp}, \tag{B3}$$

$$\boldsymbol{n}_L^{\parallel} \cdot \boldsymbol{n}_R^{\parallel} = \cos\theta_L \cos\theta_R, \tag{B4}$$

$$\boldsymbol{n}_L^{\perp} \cdot \boldsymbol{n}_R^{\perp} = \sin\theta_L \sin\theta_R \cos\gamma, \tag{B5}$$

$$\boldsymbol{n}_P \cdot (\boldsymbol{n}_L \times \boldsymbol{n}_R) = \sin\theta_L \sin\theta_R \sin\gamma. \tag{B6}$$

[1] R. Meservey, P. M. Tedrow, and P. Fulde, Phys. Rev. Lett. **25**, 1270 (1970).
[2] R. Meservey, P. M. Tedrow, and R. C. Bruno, Phys. Rev. B **11**, 4224 (1975).
[3] P. M. Tedrow and R. Meservey, Phys. Rev. Lett. **26**, 192 (1971).
[4] P. M. Tedrow and R. Meservey, Phys. Rev. B **7**, 318 (1973).
[5] D. Paraskevopoulos, R. Meservey, and P. M. Tedrow, Phys. Rev. B **16**, 4907 (1977).
[6] R. Meservey, D. Paraskevopoulos, and P. M. Tedrow, Phys. Rev. B **22**, 1331 (1980).
[7] R. Meservey and P. M. Tedrow, Phys. Rep. **238**, 173 (1994).
[8] J. S. Moodera, X. Hao, G. A. Gibson, and R. Meservey, Phys. Rev. Lett. **61**, 637 (1988).
[9] X. Hao, J. S. Moodera, and R. Meservey, Phys. Rev. B **42**, 8235 (1990).
[10] T. Tokuyasu, J. A. Sauls, and D. Rainer, Phys. Rev. B **38**, 8823 (1988).
[11] J. S. Moodera, T. S. Santos, and T. Nagahama, J. Phys.: Condens. Matter **19**, 165202 (2007).
[12] F. Hübler, J. C. Lemyre, D. Beckmann, and H. v. Löhneysen, Phys. Rev. B **81**, 184524 (2010).
[13] M. J. Wolf, C. Sürgers, G. Fischer, and D. Beckmann, Phys. Rev. B **90**, 144509 (2014).
[14] D. Beckmann, J. Phys.: Condens. Matter **28**, 163001 (2016).
[15] S. Kolenda, M. J. Wolf, and D. Beckmann, Phys. Rev. Lett. **116**, 097001 (2016).
[16] M. Silaev, P. Virtanen, F. S. Bergeret, and T. T. Heikkilä, Phys. Rev. Lett. **114**, 167002 (2015).
[17] F. S. Bergeret, M. Silaev, P. Virtanen, and T. T. Heikkilä, Rev. Mod. Phys. **90**, 041001 (2018).
[18] T. T. Heikkilä, M. Silaev, P. Virtanen, and F. S. Bergeret, Prog. Surf. Sci. **94**, 100540 (2019).
[19] A. Schmid and G. Schön, J. Low Temp. Phys. **20**, 207 (1975).
[20] P. Machon, M. Eschrig, and W. Belzig, Phys. Rev. Lett. **110**, 047002 (2013).
[21] A. Ozaeta, P. Virtanen, F. S. Bergeret, and T. T. Heikkilä, Phys. Rev. Lett. **112**, 057001 (2014).
[22] T. T. Heikkilä, R. Ojajärvi, I. J. Maasilta, E. Strambini, F. Giazotto, and F. S. Bergeret, Phys. Rev. Appl. **10**, 034053 (2018).
[23] F. Giazotto, P. Solinas, A. Braggio, and F. S. Bergeret, Phys. Rev. Appl. **4**, 044016 (2015).
[24] G. De Simoni, E. Strambini, J. S. Moodera, F. S. Bergeret, and F. Giazotto, Nano Lett. **18**, 6369 (2018).
[25] F. Giazotto and F. S. Bergeret, Appl. Phys. Lett. **102**, 132603 (2013).
[26] F. Giazotto, J. W. A. Robinson, J. S. Moodera, and F. S. Bergeret, Appl. Phys. Lett. **105**, 062602 (2014).
[27] F. Giazotto, T. T. Heikkilä, and F. S. Bergeret, Phys. Rev. Lett. **114**, 067001 (2015).
[28] M. Rouco, T. T. Heikkilä, and F. S. Bergeret, Phys. Rev. B **97**, 014529 (2018).

[29] S. Chakraborty and T. T. Heikkilä, J. Appl. Phys. **124**, 123902 (2018).

[30] E. Strambini, V. N. Golovach, G. De Simoni, J. S. Moodera, F. S. Bergeret, and F. Giazotto, Phys. Rev. Mater. **1**, 054402 (2017).

[31] X.-P. Zhang, F. S. Bergeret, and V. N. Golovach, Nano Lett. (2019).

[32] G.-X. Miao and J. S. Moodera, Appl. Phys. Lett. **94**, 182504 (2009).

[33] A. A. Abrikosov, *Fundamentals of the Theory of Metals* (Dover Publications, New York, 2017)

[34] M. G. Khusainov, Zh. Eksp. Teor. Fiz. **109**, 524 (1996) [JETP **82**, 278 (1996)].

[35] Yu. A. Izyumov, Yu. N. Proshin, and M. G. Khusainov, Phys. Usp. **45**, 109 (2002).

[36] K. Maki, Prog. Theor. Phys. **31**, 731 (1964).

[37] F. S. Bergeret, A. Verso, and A. F. Volkov, Phys. Rev. B **86**, 214516 (2012).

[38] D. N. Langenberg and A. I. Larkin, *Nonequilibrium superconductivity* (North-Holland, Amsterdam, 1986).

[39] K. D. Usadel, Phys. Rev. Lett. **25**, 507 (1970).

[40] F. S. Bergeret, A. F. Volkov, and K. B. Efetov, Phys. Rev. Lett. **86**, 4096 (2001).

[41] F. S. Bergeret, A. Verso, and A. F. Volkov, Phys. Rev. B **86**, 060506(R) (2012).

[42] R. E. Harris, Phys. Rev. B **10**, 84 (1974).

[43] A. I. Larkin and Y. N. Ovchinnikov, Zh. Eksp. Teor. Fiz. **51**, 1535 (1966) [JETP **24**, 1035 (1967)].

[44] A. Barone and G. Paterno, *Physics and Applications of the Josephson Effect* (Wiley, New York, 1982).

[45] A. Buzdin, Phys. Rev. Lett. **101**, 107005 (2008).

[46] A. Zazunov, R. Egger, T. Jonckheere, and T. Martin, Phys. Rev. Lett. **103**, 147004 (2009).

[47] A. Brunetti, A. Zazunov, A. Kundu, and R. Egger, Phys. Rev. B **88**, 144515 (2013).

[48] A. A. Reynoso, G. Usaj, C. A. Balseiro, D. Feinberg, and M. Avignon, Phys. Rev. Lett. **101**, 107001 (2008).

[49] K. N. Nesterov, M. Houzet, and J. S. Meyer, Phys. Rev. B **93**, 174502 (2016).

[50] F. Konschelle, I. V. Tokatly, and F. S. Bergeret, Phys. Rev. B **92**, 125443 (2015).

[51] F. Bergeret and I. Tokatly, Europhys. Lett. **110**, 57005 (2015).

[52] I. V. Bobkova, A. M. Bobkov, A. A. Zyuzin, and M. Alidoust, Phys. Rev. B **94**, 134506 (2016).

[53] T. Yokoyama, M. Eto, and Y. V. Nazarov, Phys. Rev. B **89**, 195407 (2014).

[54] M. A. Silaev, Phys. Rev. B **96**, 064519 (2017).

[55] M. A. Silaev, I. V. Tokatly, and F. S. Bergeret, Phys. Rev. B **95**, 184508 (2017).

[56] J.-F. Liu and K. S. Chan, Phys. Rev. B **82**, 125305 (2010).

[57] A. G. Mal'shukov, S. Sadjina, and A. Brataas, Phys. Rev. B **81**, 060502(R) (2010).

[58] Y. Lu and T. T. Heikkilä, Phys. Rev. B **100**, 104514 (2019).

[59] I. Margaris, V. Paltoglou, and N. Flytzanis, J. Phys.: Condens. Matter **22**, 445701 (2010).

[60] V. Braude and Y. V. Nazarov, Phys. Rev. Lett. **98**, 077003 (2007).

[61] A. Moor, A. F. Volkov, and K. B. Efetov, Phys. Rev. B **92**, 180506(R) (2015).

[62] R. Grein, M. Eschrig, G. Metalidis, and G. Schön, Phys. Rev. Lett. **102**, 227005 (2009).

[63] J.-F. Liu and K. S. Chan, Phys. Rev. B **82**, 184533 (2010).

[64] S. Mironov and A. Buzdin, Phys. Rev. B **92**, 184506 (2015).

[65] F. S. Bergeret, A. F. Volkov, and K. B. Efetov, Rev. Mod. Phys. **77**, 1321 (2005).

[66] V. Ambegaokar and A. Baratoff, Phys. Rev. Lett. **10**, 486 (1963).

[67] P. M. Tedrow, J. E. Tkaczyk, and A. Kumar, Phys. Rev. Lett. **56**, 1746 (1986).

[68] P. Tischer, IEEE Trans. Magn. **9**, 9 (1973).

[69] F. Jedema, H. Heersche, A. Filip, J. Baselmans, and B. Van Wees, Nature (London) **416**, 713 (2002).

[70] N. Poli, J. P. Morten, M. Urech, A. Brataas, D. B. Haviland, and V. Korenivski, Phys. Rev. Lett. **100**, 136601 (2008).

[71] A. Anthore, H. Pothier, and D. Esteve, Phys. Rev. Lett. **90**, 127001 (2003).

[72] P. G. de Gennes, *Superconductivity of Metals and Alloys*, Advanced Book Classics (Perseus, Cambridge, MA, 1999).